Friction **12**(3): 452–461 (2024)
https://doi.org/10.1007/s40544-023-0770-6
ISSN 2223-7690
CN 10-1237/TH

RESEARCH ARTICLE

Molecular design of recyclable thermosetting polyimide and its composite with excellent mechanical and tribological properties

Xiaoyue WANG[1,2,3], Zenghui YANG[1], Tingmei WANG[1,2], Qihua WANG[1,2,3], Xinrui ZHANG[1,*], Song LI[1,*]

[1] *Key Laboratory of Science and Technology on Wear and Protection of Materials, Lanzhou Institute of Chemical Physics, Chinese Academy of Sciences, Lanzhou 730000, China*

[2] *Center of Materials Science and Optoelectronics Engineering, University of Chinese Academy of Sciences, Beijing 100049, China*

[3] *State Key Laboratory of Solid Lubrication, Lanzhou Institute of Chemical Physics, Chinese Academy of Sciences, Lanzhou 730000, China*

Received: 17 September 2022 / Revised: 15 February 2023 / Accepted: 21 April 2023

Abstract: Recyclability of thermosetting polymers and their composites is a challenge for alleviating environmental pollution and resource waste. In this study, solvent-recyclable thermosetting polyimide (PI) and its composite were successfully synthesized. The tensile strength, elongation at break, and Young's modulus of PI are 108.70 ± 7.29 MPa, 19.35% ± 3.89%, and 2336.42 ± 128.00 MPa, respectively. The addition of reduced graphene oxide (RGO) not only enhances the mechanical properties of PI but also endows it with excellent tribological properties. The PI illustrates a high recycling efficiency of 94.15%, but the recycled composite exhibits inferior mechanical properties. The recycling and utilization of PI and its composite are realized through imine bonds (–C=N), which provides new guidance for solving the problem of environmental pollution and resource waste and is potential application in the field of sustainable tribology.

Keywords: thermosetting polyimide (PI); recyclability; dynamic covalent bonds; friction and wear; polymer composites

1 Introduction

Friction and wear consume more than 1/3 of the global primary energy and are one of the leading reasons for material damage and failure [1–3]. Therefore, the design and preparation of high-performance lubricating materials are important consideration in the field of tribology. Compared with metallic materials and inorganic nonmetallic materials, polymers and their composites have attracted numerous attention due to flexible structural design, great thermal stability, and excellent self-lubricating properties [4–6]. Among them, thermosetting polyimide (PI) with outstanding solvent resistance, mechanical properties, and bearing capacity plays an irreplaceable role in mechanical moving parts, aerospace and transportation [7–9]. PI shows a poor tribological performance when used alone in severe working environments and needs to incorporate functional fillers to enhance its tribological and mechanical properties. Numerous researches have shown that two-dimensional (2D) nanosheets, such as titanium carbide, hexagonal boron nitride, and graphene oxide, are widely used in solid lubrication [10–13]. Among 2D layered nanomaterials, reduced graphene oxide (RGO) has become a potential lubricant additive owing to its excellent thermal conductivity, good surface activity and self-lubricating performance [14–16]. The incorporation of RGO can significantly enhance the tribological and mechanical properties of PI.

However, thermosetting PI with a permanent cross-linked 3D network cannot achieve the characteristics of thermoplastic polymer recycling, remolding or reprocessing and is mainly disposed of

* Corresponding authors: Xinrui ZHANG, E-mail: xruiz@licp.cas.cn; Song LI, E-mail: lisong@licp.cas.cn

by landfill and incineration, which causes serious resources waste and environmental pollution [17]. The postprocessing of PI has always been a problem and challenge because of the rigid structure main chain, strong intermolecular interactions and high symmetry [18, 19]. Therefore, breaking the unsustainable linear mode of PI and its composite, preparing recyclable composites with closed-loop cycles, and realizing the recycling of functional fillers and resin matrices are one of the key research topics in the field of sustainable tribology.

In recent years, dynamic covalent bonds have been introduced into thermosetting polymers through molecular design, realizing the recycling and reuse of thermosetting polymers [20–22]. Dynamic covalent bonds (disulfide bonds [23, 24], –C=N bonds [25, 26], Diels–Alder bonds [27, 28], boronic ester bonds [29, 30], etc.) can dissociate and recombine through the movement of molecular chains under appropriate conditions to achieve topological rearrangement. The emergence of dynamic covalent bonds provides a new solution to the problem of recycling and remolding of traditional thermosetting polymers. Our team took advantage of the dynamic properties of –C=N to acids and reported a fully closed-loop recyclable thermosetting PI by solvent without any catalyst [31]. Wan et al. [32] introduced –C=N into PI and obtained a recycled and self-healed PI. The above works make a great contribution to the recyclability of PI. However, there are few reports on the recycling of PI composite and the tribological properties of the materials before and after recycling.

In the present work, PI was synthesized by reacting amine-terminated bisimide (ATBI) with 1,3,5-benzenetricarboxaldehyde (BTA) and possessed the dynamic properties of –C=N bonds to acids. Meanwhile, the PI composite reinforced by RGO was also prepared and named PI–RGO. The chemical structure, mechanical and tribological properties, and recycling efficiency of the PI and PI–RGO were characterized before and after recycling. The results demonstrated that PI has excellent mechanical properties and high recycling efficiency, and RGO could enhance the tribological properties of the PI composite. Compared to recycled PI (RPI), the main reason for the performance decline of recycled PI–RGO (RPI–RGO) is the agglomeration of functional fillers. Recyclable thermosetting PI and PI–RGO have broad application prospects in the field of sustainable tribology, and we believe this work is instructive for the recycling and application of polymers and their composites.

2 Materials and methods

2.1 Materials

2,2-bis(4-(3,4-dicarboxyphenoxy)phenyl)propane dianhydride (BPADA), 4,4′-Oxydianiline (ODA), and 1,3,5-benzenetricarboxaldehyde (BTA) were purchased from TCI Chemicals Co., Ltd. N-Methyl-2-pyrrolidone (NMP) was obtained from Shanghai Kefeng Industry & Commerce Co., Ltd. Dichloromethane (DCM), hydrochloric acid (HCl), toluene and ethanol were supplied by Rionlon Bohua (Tianjin) Pharmaceutical & Chemical Co., Ltd. The RGO was prepared by the following work [33], and the corresponding transmission electron microscope (TEM), Raman and Fourier transform infrared are shown in Figs. S1–S3 in the Electronic Supplementary Material (ESM).

2.2 Synthesis of ATBI

The synthetic route of ATBI refers to the previous work of our group [31]. ODA (2.00 g, 10.00 mmol) was placed in a three-neck flask filled with NMP solvent under N_2 atmosphere with uninterrupted stirring until the solution was clear in an ice water bath. Then, BPADA (2.60 g, 5.00 mmol) was added to the above solution and reacted for 24 h. After that, a Dean-Stark device containing toluene was inserted into the three-neck flask and placed into an electric heating jacket at 220 °C for 6 h to remove water. Next, the solution in the three-neck flask was poured into ethanol and then filtered and dried in an oven at 80 °C overnight. Finally, the light-yellow products were obtained.

2.3 Synthesis of PI

ATBI (0.90 g, 1.00 mmol) was dissolved into NMP (3.00 mL) and mixed with BTA (0.10 g, 0.67 mmol) that dispersed into DMF (3.60 mL) until the solution became homogeneous. The mixed solution was spread onto the glass after stirring well and then put into

an oven at 80 °C to remove solvent for 12 h. Next, the temperature was programmed at 200 °C for an hour, 250 °C for an hour and 300 °C for 1 h to further crosslink. A transparent PI thin film was obtained.

2.4 Synthesis of PI–RGO

RGO (0.10 g) was dissolved into ATBI solution, which was prepared by dispersing ATBI (0.90 g, 1.00 mmol) in NMP (3.00 mL) under continuous ultrasound until RGO was evenly dispersed. After that, BTA solution that was prepared by dissolving BTA (0.10 g, 0.67 mmol) in DMF (3.60 mL) was added to the ATBI solution. The next step is the same as the synthesis of PI.

2.5 Characterization

Nuclear magnetic resonance (NMR) spectra were obtained on a Bruker 400 MHz spectrometer (Switzerland) at room temperature, and deuterated dimethyl sulfoxide (DMSO-d_6) was chosen as the solvent. Gel permeation chromatography (GPC, PL-GPC50) was used to measure the number-average molecular weight (M_n) using tetrahydrofuran as the solvent. Fourier transform infrared (FTIR) spectroscopy of samples were taken on a Bruker Nicolet Nexus 870 spectrometer (Germany) from 4,000 to 500 cm^{-1} with a mold of attenuated total reflection attachment. Mechanical properties were tested on an electronic universal tensile testing machine (Shimadzu, AG-X) for dumbbell-shaped (30 mm × 2 mm × 0.1 mm) samples at a tensile rate of 10 mm·min^{-1} according to ISO527-2/1BB. Surface images and elemental distribution were measured by field emission scanning electron microscope with energy dispersive spectrometer (FE-SEM/EDS, Quanta 650 FEG FEI). Transmission electron microscope (TEM, FEI Tecnai F20) was used to characterize the microscopic topography of RGO. LabRAM HR evolution (HORIBA Jobin Yvon S.A.S.) was used to test the Raman spectrum of RGO with a 532 nm laser. Super depth of field confocal 3D Profiler (UP-Lambda, Rtec-Instruments) was applied to review and calculate the cross-section profiles and areas of wear scars.

The recycling of PI was achieved by adding shredded PI pieces to the mixed solution of NMP and DCM, followed by the addition of HCl. After the PI pieces were completely decomposed, the mixed solution was poured on the glass, and the temperature was programmed to increase as "Synthesis of PI". Finally, the recycled PI film was obtained. The recycling steps of PI–RGO are the same as those of PI. The recycling efficiency (η_r) was calculated by Eq. (1):

$$\eta_r = \sigma_r / \sigma_0 \times 100\% \quad (1)$$

where σ_0 is the tensile strength of the original PI or PI–RGO, and σ_r is the tensile strength of RPI or RPI–RGO.

The tribological experiments were implemented on a reciprocating tribometer (CSM, Switzerland) at room temperature. The schematic diagram of the contact configuration of the friction pairs was displayed in Scheme S1. The counterpart ball, load and sliding speed were GCr15 (GB/T 18254-2002, HRC 62, Φ = 3 mm), 3 N and 3 cm/s. Each test lasted 2 h and was repeated at least three times. The friction coefficient was measured online, and the wear rate (W, mm^3/(N·m)) was calculated according to Eq. (2):

$$W = SL_1/PL \quad (2)$$

where S, L_1, P, and L are cross-sectional area, wear scar length, load, and sliding distance, respectively.

3 Results and discussion

3.1 Synthesis and characterization of ATBI, PI, and PI–RGO

The synthetic route of ATBI is displayed in Scheme S2 in the ESM. ODA and BPADA were dissolved in NMP and reacted in an ice water bath for 24 h under N_2 atmosphere, and then water was removed at 220 °C for 6 h. The reaction solution was poured into ethanol, and light-yellow substances were precipitated, filtered, and dried in an oven at 80 °C overnight to obtain ATBI. The qualitative characterization was carried out by NMR (^{1}H NMR (400 MHz, DMSO) δ 7.96 (s, 1H), 7.46 (s, 1H), 7.40 (s, 2H), 7.34 (s, 1H), 7.23 (s, 2H), 7.13 (s, 2H), 6.97 (s, 2H), 6.83 (s, 2H), 6.62 (s, 2H), 5.04 (s, 2H), 1.72 (s, 3H)) as shown in Fig. S4 in the ESM. Figure S5 in the ESM illustrates the functional groups of ATBI in which the vibration peaks of –C–N appear at 1,380 and 1,240 cm^{-1}. The characteristic absorption peaks at 3,461 and 3,376 cm^{-1} are attributed to stretching

vibration of $-NH_2$. In addition, the peaks at 1,774 and 1,720 cm^{-1} agree with the asymmetric and symmetric stretching vibrations of –C=O. In addition, the M_n (≈ 902) of ATBI is acquired through GPC analysis and is consistent with the theoretical value. The above results fully indicate that the ATBI has been prepared successfully.

Next, the stoichiometric amounts of amino-terminated ATBI solution were mixed with aldehyde-terminated BTA solution and further reacted under temperature-programmed conditions to obtain a PI film, whose detailed preparation process is shown in Scheme 1. Figure 1 demonstrates the FTIR spectrum of ATBI, BTA, and PI. The characteristic peaks at 3,461 and 3,376 cm^{-1} of $-NH_2$ as well as 1,700 cm^{-1} of –CH=O disappear with the emergence of a new peak (1,620 cm^{-1}) that corresponds to the –C=N bond [31], which proves that ATBI successfully reacts with BTA. The PI composite reinforced by RGO is abbreviated as PI–RGO, whose preparation process is displayed in Scheme 1. RGO was dissolved in ATBI solution and mixed with BTA, and the subsequent processing steps were the same as those for the synthesis of PI. Here, RGO was chosen as the functional filler because of its excellent lubricating properties. The corresponding results reveal that RGO has a large number of functional groups on the surface, which is beneficial for improving its dispersion in PI. In addition, the FTIR spectrum of PI–RGO is the same as that of PI, indicating that the addition of RGO cannot affect the –C=N structure of the original PI.

3.2 Mechanical and tribological properties of PI and PI–RGO

The excellent mechanical properties and self-lubricating performance of polymers and their composites are the key to wide application in aerospace, chemical and pharmaceutical, textile and precision machinery industries [34–36]. Therefore, the mechanical and tribological properties of PI and PI–RGO were systematically explored. The mechanical properties of PI and PI–RGO were measured by an electronic universal tensile testing machine. Typical tensile curves are shown in Fig. 2(a). The PI is provided with

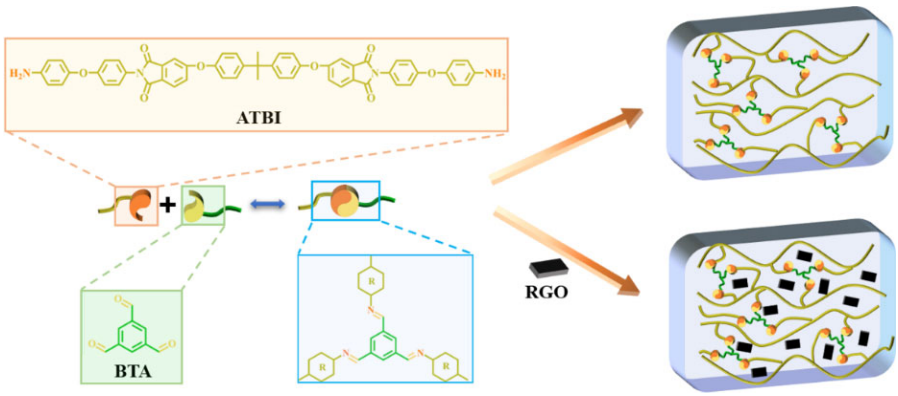

Scheme 1 Synthetic route of PI and PI–RGO.

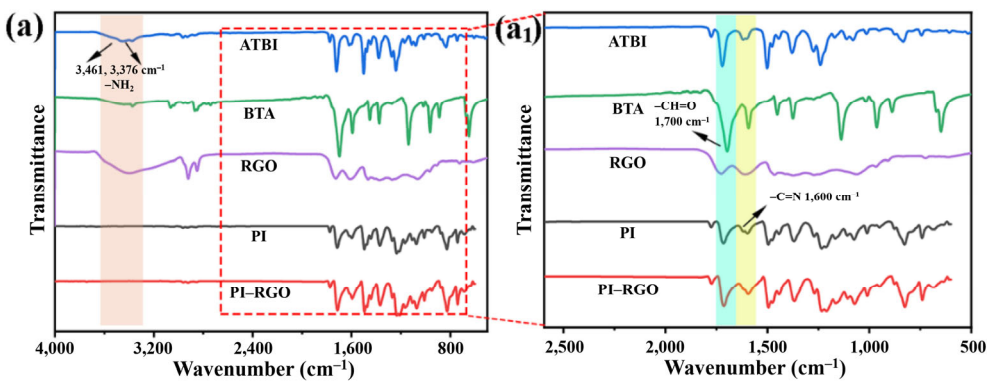

Fig. 1 FT-IR spectrum of ATBI, BTA, RGO, PI, and PI–RGO.

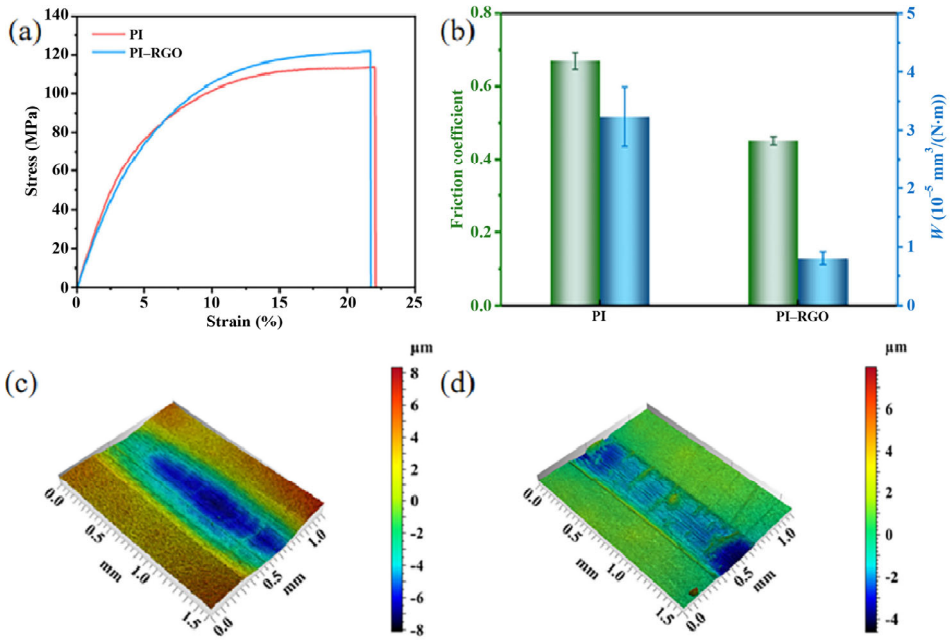

Fig. 2 (a) Typical stress–strain curves of PI and PI–RGO. (b) Variation in the friction coefficient and wear rate of PI and PI–RGO. 3D morphologies of wear scars of (c) PI and (d) PI–RGO.

tensile strength of 108.70 ± 7.29 MPa, break strain of 19.35% ± 3.89%, and Young's modulus of 2336.42 ± 128.00 MPa. The excellent properties come from cross-linked structures, which are from the reaction of ATBI and BTA. For PI–RGO, the RGO are uniformly dispersed in the NMP and DMF without anymohen as shown in Fig. S6 in the ESM. This phenomenon strongly indicates that RGO has excellent compatibility with solvents, which can enhance the dispersion of GRO in PI. As shown in Fig. 2(a), PI–RGO shows a higher tensile strength (117.87 ± 3.65 MPa) compared with PI because molecular chain movement is limited by RGO and requires more force to make the chains move. Figure 2(b) illustrates the variation of tribological properties of PI and PI–GRO. The friction coefficient and wear rate of PI are 0.67 and 3.23×10^{-5} $mm^3/(N\cdot m)$, respectively. PI–RGO exhibits a lower friction coefficient (0.40) and wear rate (0.80×10^{-5} $mm^3/(N\cdot m)$). Compared with PI, the friction coefficient and wear rate of PI–RGO are reduced by 40.30% and 75.23%, respectively. Figures 2(c) and 2(d) demonstrate the three-dimensional (3D) topographies of the wear scars. The 3D images display that the wear resistance of PI–RGO is significantly better than that of PI, which is in full agreement with the results in Fig. 2(b). The reason for the above results is that the RGO easily slips and shears owing to the layered structure with the weak Van der Waals forces.

3.3 Recyclability of PI and PI–RGO

The pH sensitivity of the –C=N bond enables dynamic reversible reaction, as shown in Fig. 3(a). For PI, small fragments were placed in a glass bottle containing NMP and DCM (the volume ratio of NMP and DCM was 3:7). And HCl (6% to the mixed solvents) was added dropwise into it. Because the –C=N bond gradually dissociated in the acidic environment, the color of the mixed solution gradually deepened. After the PI was completely decomposed, the mixed solution turned dark brown, as shown in Fig. 3(b). Subsequently, the mixed solution was poured on the glass, and the temperature was programmed to increase as "Synthesis of PI". Finally, RPI film was successfully obtained. Next, PI–RGO was recycled with the same method, as shown in Fig. 3(c), in which the mixed solution turned completely black after dissociation because of the existence of RGO.

Figure 4(a) displays the FTIR spectrum of PI and PI–RGO before and after recycling to explore the structural consistency. FTIR spectra indicates that there is no change in the functional groups of the PI, RPI, PI–RGO and RPI–RGO, suggesting that the

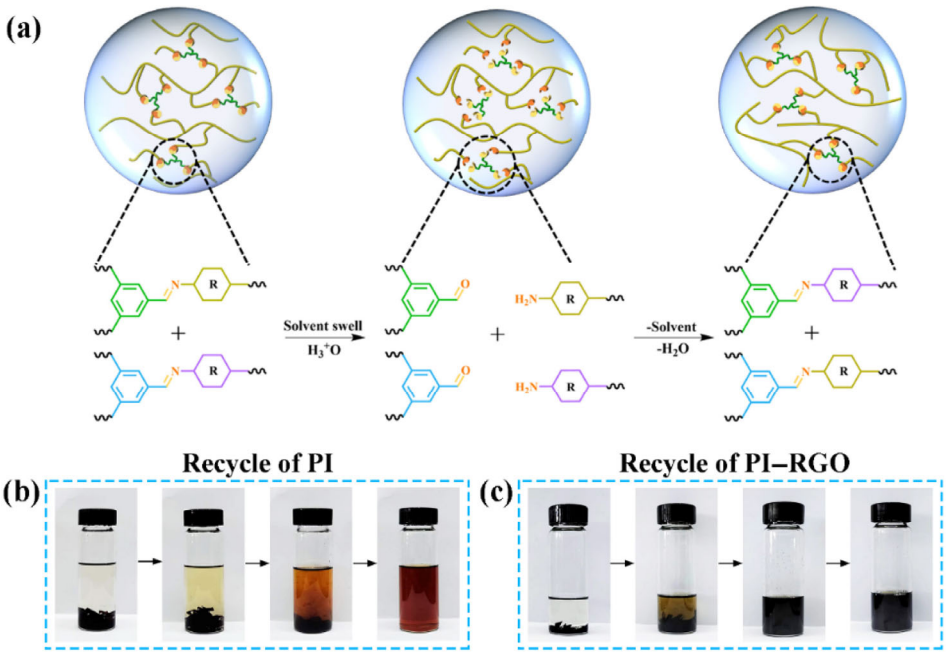

Fig. 3 (a) Dissociation and association mechanism of PI recycling. The dissociation process of (b) PI and (c) PI–RGO in an acidic environment.

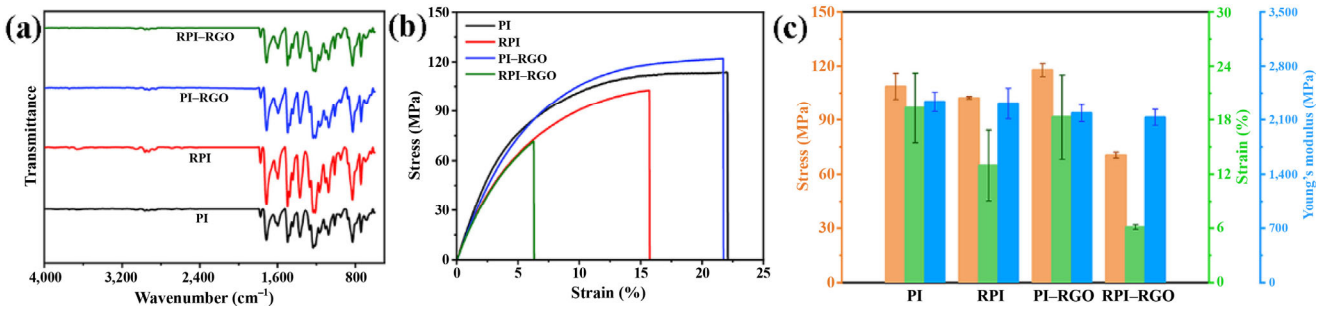

Fig. 4 (a) FTIR spectra, (b) stress–strain curves and (c) stress, strain, and Young's modulus of PI, RPI, PI–RGO, and RPI–RGO.

aldehyde-amine reaction is relatively thorough. In addition, the mechanical properties of RPI were measured and compared with original PI (see Figs. 4(b) and 4(c)). The corresponding results indicate that RPI displays relatively low mechanical properties (tensile strength of 102.34 ± 0.72 MPa, break strain of 12.98% ± 3.90%, and Young's modulus of 2314.84 ± 200.73 MPa). This is because the acidic environment destroys part of the amino groups generated after acid hydrolysis of PI, and the cross-linking density decreases. According to formula 1, the calculated recovery efficiency of PI is 94.15%.

Compared with PI–RGO, the mechanical properties of RPI–RGO decreased significantly, exhibiting a tensile strength of only 70.50 ± 1.65 MPa, break strain of 6.12% ± 0.27%, and Young's modulus of 2132.14 ± 104.08 MPa. To explore the reasons for the decline in mechanical properties, the fracture surfaces of PI–RGO and RPI–RGO were analyzed by SEM. The results demonstrate that microstructure of the PI–RGO's fracture surface is uniform (see Fig. 5(a)). However, the fracture morphology of RPI–RGO is completely different from that of PI–RGO, and an uneven microscopic morphology is clearly observed, as shown in Fig. 5(b). The microstructure of the top half of the RPI–RGO is similar to PI-RGO (see Fig. 5(b_1)), but the morphology of the bottom half is granular with an obvious delamination, as shown in Fig. 5(b_2). EDS analysis provides the distribution of C elements in the fracture surfaces. It is clearly found that the C element distribution of RPI–RGO is not uniform compared with PI–RGO, as displayed in Figs. 5(a_2)

and 5(b_3). The agglomeration phenomenon of RGO is the root cause of the degradation of mechanical and tribological properties. To verify this statement, RGO was placed in glass bottles containing NMP, DCM, and the mixed solution of NMP and DCM, respectively. The RGO was still mixed evenly in NMP or DCM after 6 h, but the stratification occurred in the mixed solution (see Fig. S7 in the ESM). PI–RGO was also dissolved in the mixed solution of NMP and DCM during the recovery process, which led to the aggregation of RGO and decrease in mechanical properties. Meanwhile, the friction and wear behaviors of RPI and RPI–RGO were also investigated. Figure 6(a) shows the change in the friction coefficient and wear rate before and after PI and PI–RGO recycling. The results demonstrate that the friction coefficient of the recycled PI decreases significantly, but the wear rate shows an increasing trend. The main reason is that the acidic environment during the recycling process reduces the cross-linking density of PI. Therefore, the polymer chains are more easily sheared, and the molecular chains are prone to orientate movement

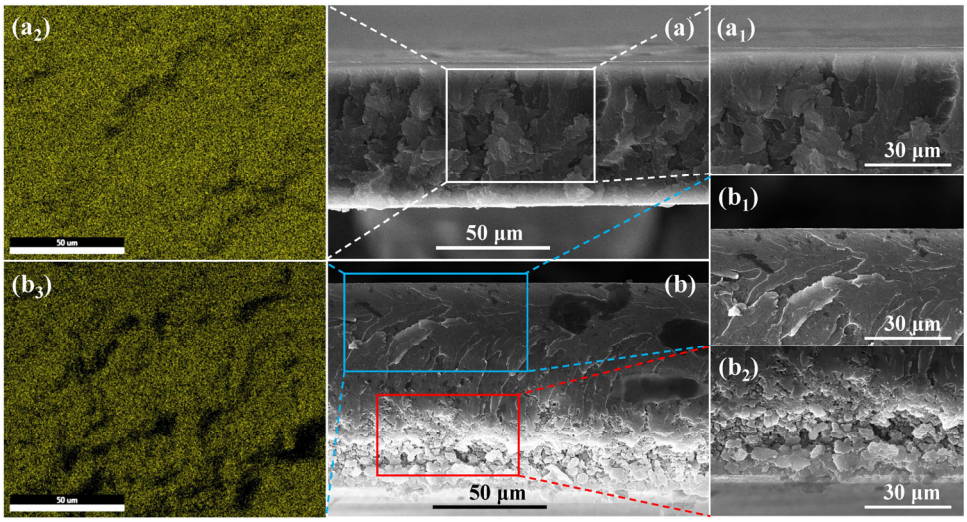

Fig. 5 (a) Cross-sectional morphology of PI–RGO, (a_1) corresponding partially enlarged morphology and (a_2) element mapping maps of C. (b) Cross-sectional morphology of RPI–RGO, corresponding to partially enlarged morphology (b_1) top half and (b_2) bottom half, as well as (b_3) element mapping maps of C.

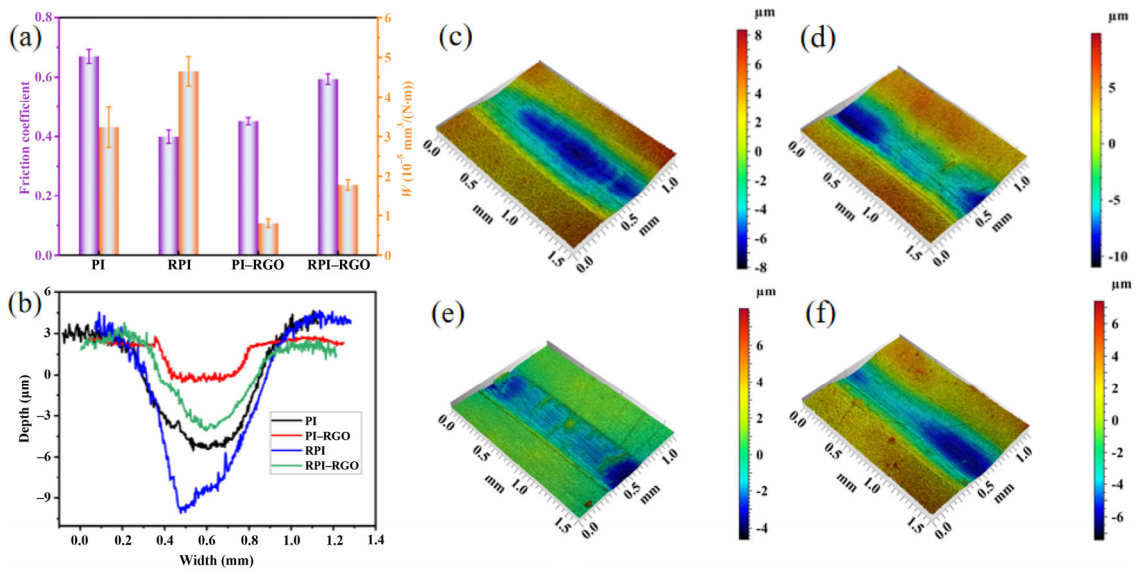

Fig. 6 (a) Variation in the friction coefficient and wear rate. (b) The cross-section profiles of wear tracks. 3D morphologies of wear scars of (c) PI, (d) RPI, (e) PI–RGO, and (f) RPI–RGO.

along the sliding direction under the action of friction, which reduces the friction coefficient. The reduced density of cross-linking results in the polymer being more susceptible to abrasion. Different from the change of tribological properties before and after PI recycling, the friction coefficient and wear rate of RPI–RGO show an increasing phenomenon. The wear cross-section curve can intuitively reflect the wear resistance of the material. The RGO can improve the wear resistance of PI, as shown in Fig. 6(b). However, the wear resistance of both RPI and RPI–RGO decreases. Figures 6(c)–6(f) illustrate the 3D wear scars of PI, RPI, PI–RGO, and RPI–RGO, respectively. The variation trend of the width and height of the wear scars was the same as that of the wear rate. The main reason for the change in tribological properties before and after recycling is the reduction of cross-linking density and agglomeration of RGO.

4 Conclusions

In this work, we synthesized recyclable polyimide (PI) and PI–reduced graphene oxide (RGO) and explored the tribological properties of PI and PI–RGO before and after recycling for the first time. Both of PI and PI–RGO show excellent mechanical properties, and PI–RGO exhibits a higher strength (117.87 ± 3.65 MPa) than PI (108.70 ± 7.29 MPa) due to the movement of molecular chains is limited by RGO. Meanwhile, RGO reduces the friction coefficient and wear rate by 40.30% and 75.23% compared to PI. The existence of –C=N bonds endow PI and PI–RGO recyclability without metal catalysts or complicated hot-pressing processes. The recycled PI (RPI) shows a lower strength (102.34 ± 0.72 MPa) and wear resistance (4.65×10^{-5} $mm^3/(N\cdot m)$) than PI (108.70 ± 7.29 MPa, 3.23×10^{-5} $mm^3/(N\cdot m)$) owing to the decrease of cross-linking density, and the η_r is 94.15%. The mechanical properties and tribological performance of RPI–RGO greatly decrease due to the aggregation of RGO. We anticipate that this work expands the application and development of recyclable materials in the field of tribology, and we have opened a door for composites recycling and green tribology. In the future, we will continue to study the effect of acidity on recycling and solve the performance problems of composites after recycling.

Acknowledgements

This work was financially supported by the Natural Science Foundation of Gansu Province (Grant No. 22JR5RA108), the National Natural Science Foundation of China (Grant No. 52205234), the Youth Innovation Promotion Association of Chinese Academy of Sciences (Grant No. Y2018457), and the Key Program of the Lanzhou Institute of Chemical Physics, CAS (Grant No. KJZLZD-3).

Declaration of competing interest

The authors have no competing interests to declare that are relevant to the content of this article.

Electronic Supplementary Material: Supplementary material is available in the online version of this article at https://doi.org/10.1007/s40544-023-0770-6

References

[1] Holmberg K, Erdemir A. Influence of tribology on global energy consumption, costs and emissions. *Friction* **5**(3): 263–284 (2017)

[2] Myshkin N, Kovalev A. Adhesion and surface forces in polymer tribology—A review. *Friction* **6**(2): 143–155 (2018)

[3] Liu L, Zhou M, Jin L, Li L, Mo Y, Su G, Li X, Zhu H, Tian Y. Recent advances in friction and lubrication of graphene and

other 2D materials: Mechanisms and applications. *Friction* **7**(3): 199–216 (2019)

[4] Imani A, Zhang H, Owais M, Zhao J, Chu P, Yang J, Zhang Z. Wear and friction of epoxy based nanocomposites with silica nanoparticles and wax-containing microcapsules. *Composites Part A: Appl Sci Manuf* **107**: 607–615 (2018)

[5] Yuan J, Zhang Z, Yang M, Wu L, Li P, Guo F, Men X, Liu W. Coupling hybrid of BN nanosheets and carbon nanotubes to enhance the mechanical and tribological properties of fabric composites. *Composites Part A: Appl Sci Manuf* **123**: 132–140 (2019)

[6] Guo L, Li G, Guo Y, Zhao F, Zhang L, Wang C, Zhang G. Extraordinarily low friction and wear of epoxy-metal sliding pairs lubricated with ultra-low sulfur diesel. *ACS Sustainable Chem Eng* **6**: 15781–15790 (2018)

[7] Samyn P, Schoukens G, De Baets P. Micro- to nanoscale surface morphology and friction response of tribological polyimide surfaces. *Appl Surf Sci* **256**: 3394–3408 (2010)

[8] Samyn P, Quintelier J, Schoukens G, De Baets P. The sliding behaviour of sintered and thermoplastic polyimides investigated by thermal and Raman spectroscopic measurements. *Wear* **264**: 869–876 (2008)

[9] Tanaka A, Umeda K, Takatsu S. Friction and wear of diamond-containing polyimide composites in water and air. *Wear* **257**: 1096–1102 (2004)

[10] Zeng X, Peng Y, Yu M, Lang H, Cao X, Zou K. Dynamic sliding enhancement on the friction and adhesion of graphene, graphene oxide, and fluorinated graphene. *ACS Appl Mater Interfaces* **10**: 8214–8224 (2018)

[11] Xu D, Wang C, Espejo C, Wang J, Neville A, Morina A. Understanding the friction reduction mechanism based on molybdenum disulfide tribofilm formation and removal. *Langmuir* **34**: 13523–13533 (2018)

[12] Tocci G, Joly L, Michaelides A. Friction of water on graphene and hexagonal boron nitride from ab initio methods: Very different slippage despite very similar interface structures. *Nano Lett* **14**: 6872–6877 (2014)

[13] Lian W, Mai Y, Liu C, Zhang L, Li S, Jie X. Two-dimensional Ti3C2 coating as an emerging protective solid-lubricant for tribology. *Ceram Int* **44**: 20154–20162 (2018)

[14] Liu Y, Shin D G, Xu S, Kim C L, Kim D E. Understanding of the lubrication mechanism of reduced graphene oxide coating via dual in-situ monitoring of the chemical and topographic structural evolution. *Carbon* **173**: 941–952 (2021)

[15] Kim H J, Kim D E. Water lubrication of stainless steel using reduced graphene oxide coating. *Sci Rep* **5**: 17034 (2015)

[16] Larsson E, Westbroek R, Leckner J, Jacobson S, Rudolphi Å K. Grease-lubricated tribological contacts-Influence of graphite, graphene oxide and reduced graphene oxide as lubricating additives in lithium complex (LiX)-and polypropylene (PP)-thickened greases. *Wear* **486**: 204107–204120 (2021)

[17] Hong M, Chen E Y X. Future directions for sustainable polymers. *Trends in Chem* **1**: 148–151 (2019)

[18] Yi C, Li W, Shi S, He K, Ma P, Chen M, Yang C. High-temperature-resistant and colorless polyimide: Preparations, properties, and applications. *Solar Energy* **195**: 340–354 (2020)

[19] Ji D, Li T, Hu W, Fuchs H. Recent progress in aromatic polyimide dielectrics for organic electronic devices and circuits. *Adv Mater* **31**: 1806070–1806088 (2019)

[20] Christensen P R, Scheuermann A M, Loeffler K E, Helms B A. Closed-loop recycling of plastics enabled by dynamic covalent diketoenamine bonds. *Nat Chem* **11**: 442–448 (2019)

[21] Jin Y, Lei Z, Taynton P, Huang S, Zhang W. Malleable and recyclable thermosets: The next generation of plastics. *Matter* **1**: 1456–1493 (2019)

[22] Zheng N, Xu Y, Zhao Q, Xie T. Dynamic covalent polymer networks: A molecular platform for designing functions beyond chemical recycling and self-healing. *Chem Rev* **121**: 1716–1745 (2021)

[23] Zhang Q, Shi C Y, Qu D H, Long Y T, Feringa B L, Tian H. Exploring a naturally tailored small molecule for stretchable, self-healing, and adhesive supramolecular polymers. *Sci Adv* **4**: 8192–8200 (2018)

[24] Yao W, Tian Q, Shi J, Luo C, Wu W. Printable, down/up-conversion triple-mode fluorescence responsive and colorless self-healing elastomers with superior toughness. *Adv Funct Mater* **31**: 2100211–2100221 (2021)

[25] Gao S, Cheng Z, Zhou X, Liu Y, Wang J, Wang C, Chu F, Xu F, Zhang D. Fabrication of lignin based renewable dynamic networks and its applications as self-healing, antifungal and conductive adhesives. *Chem Eng J* **394**: 124896–124905 (2020)

[26] Geng H, Wang Y, Yu Q, Gu S, Zhou Y, Xu W, Zhang X, Ye D. Vanillin-based polyschiff vitrimers: Reprocessability and chemical recyclability. *ACS Sustainable Chem Eng* **6**: 15463–15470 (2018)

[27] Schäfer S, Kickelbick G. Double reversible networks: Improvement of self-healing in hybrid materials via combination of Diels-Alder cross-linking and hydrogen bonds. *Macromolecules* **51**: 6099–6110 (2018)

[28] Wu P, Cheng H, Wang X, Shi R, Zhang C, Arai M, Zhao F. A self-healing and recyclable polyurethane-urea Diels-Alder

adduct synthesized from carbon dioxide and furfuryl amine. *Green Chem* **23**: 552–560 (2021)

[29] An H, Bo Y, Chen D, Wang Y, Wang H, He Y, Qin J. Cellulose-based self-healing hydrogel through boronic ester bonds with excellent biocompatibility and conductivity. *RSC Adv* **10**: 11300–11310 (2020)

[30] Chen Y, Tang Z, Zhang X, Liu Y, Wu S, Guo B. Covalently cross-linked elastomers with self-healing and malleable abilities enabled by boronic ester bonds. *ACS Appl Mater Interfaces* **10**: 24224–24231 (2018)

[31] Yang Z, Zhang Y, Li S, Zhang X, Wang T, Wang Q. Fully closed-loop recyclable thermosetting shape memory polyimide. *ACS Sustainable Chem Eng* **8**: 18869–18878 (2020)

[32] Wan B, Zheng M S, Yang X, Dong X, Li Y, Mai Y W, Chen G, Zha J W. Recyclability and self-healing of dynamic cross-linked polyimide with mechanical/electrical damage. *Energy Environ Mater* **6**: e12427 (2022)

[33] Gao W, Chen H, Cao J, Chen S, Ma Y, Chen Q, Zhu B, Jia J, Huang A, Bai Y. Size effect on the high-strength and electrically conductive polyolefin/reduced graphene oxide (RGO) composites. *J Phys Chem C* **122**: 7968–7974 (2018)

[34] Kuang X, Guo E, Chen K, Qi H J. Extraction of biolubricant via chemical recycling of thermosetting polymers. *ACS Sustainable Chem Eng* **7**: 6880–6888 (2019)

[35] Yin N, Xing Z, He K, Zhang Z. Tribo-informatics approaches in tribology research: A review. *Friction* **11**(1): 1–22 (2023)

[36] Kumara C, Speed L, Viola M B, Luo H, Qu J. Using ionic liquid additive to enhance lubricating performance for low-viscosity engine oil. *ACS Sustainable Chem Eng* **9**: 7198–7205 (2021)

Xinrui ZHANG. He received his Ph.D. degree in physical chemistry from Lanzhou Institute of Chemical Physics, Chinese Academy of Sciences in 2010. Now, he is a professor at the Key Laboratory of Science and Technology on Wear and Protection of Materials, Lanzhou Institute of Chemical Physics, Chinese Academy of Sciences. He has authored or co-authored more than 50 journal papers. His research interests include: (1) high strength and shape memory polyurethane; (2) design, preparation and wear failure mechanism of polymer-based lubrication and sealing materials; and (3) type selection design and service behavior research of sealing composite components.

Song LI. He received his Ph.D. degree in materials science from Lanzhou Institute of Chemical Physics, Chinese Academy of Sciences, Beijing, China in 2021. Now, he is working as a researcher in the Key Laboratory of Science and Technology on Wear and Protection of Materials, Lanzhou Institute of Chemical Physics, Chinese Academy of Sciences. His research interests include special engineering plastics, polymer tribology, and functional polymers and their composites.

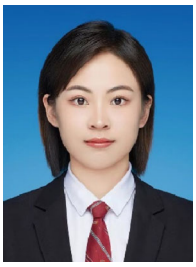

Xiaoyue WANG. She received her B.S. degree from Liaocheng University. Now, she is a Ph.D. candidate in the Lanzhou Institute of Chemical Physics, Chinese Academy of Sciences, University of Chinese Academy of Sciences. Her research is focused on the high-performance dynamic elastomers and polymers tribology.